Nuclear Instruments and Methods in Physics Research A 374 (1996) 118–126

NUCLEAR INSTRUMENTS & METHODS IN PHYSICS RESEARCH Section A

ELSEVIER

A high precision magnetometer based on pulsed NMR

R. Prigl[a,1,*], U. Haeberlen[b], K. Jungmann[a], G. zu Putlitz[a], P. von Walter[a]

[a] *Physikalisches Institut, Universität Heidelberg, D-69120 Heidelberg, Germany*
[b] *Max Planck Institut für Medizimische Forschung, D-69120 Heidelberg, Germany*

Received 27 December 1995

Abstract

A magnetometer based on pulsed proton magnetic resonance has been developed and constructed. The system will be employed for an accurate measurement of the absolute magnetic field in the region of 1.45 T in a precision experiment on the muon's anomalous magnetic moment at the Brookhaven National Laboratory (BNL, USA), where a knowledge of the magnetic field is required with 1×10^{-7} relative accuracy. The performance of the magnetometer has been tested in a large bore superconducting magnet and a precision of one part in 10^8 was achieved.

1. Introduction

The method of **n**uclear **m**agnetic **r**esonance (NMR) has been employed for measuring magnetic fields in many precision experiments [1]. Due to its capability of determining absolute field values, it is also commonly used for the calibration of magnetic sensors which are based on other physical principles such as, e.g., Hall plates [2]. The high resolution of NMR magnetometers arises from the sharp resonance lines observed in many liquid or gaseous samples containing nuclei with nonzero spin. Even in some solids, especially polymers, the residual dynamics of the molecules can average out line broadening interactions to a great extent. Thus commercial NMR magnetometers (e.g., Teslameter PT2025, Metrolab, Switzerland) with rubber samples have resolutions in the sub-ppm range in magnetic fields of the order of 1 T. New precision experiments currently in progress, however, require the knowledge of the magnitude of magnetic fields to an accuracy one order of magnitude beyond the capability of commercial instruments. The magnetometer described in this article has been developed to meet the specifications of the new experiment AGS 821 at the Brookhaven National Laboratory (BNL), Upton, New York, USA [3], which aims to improve the experimental accuracy of the g-factor of the muon, respectively its magnetic anomaly $a_\mu = (g_\mu - 2)/2$ by a factor of 20. This experiment has the potential of revealing contributions to the magnetic anomaly a_μ from physics beyond the standard model. It requires the measurement of a magnetic field of about 1.45 T in a storage ring of 7.112 m radius inside the toroidal storage volume of radius $\rho =$ 4.5 cm [4] to a relative accuracy of 0.1 ppm. For online field measurements, a repeatability of 5 parts in 10^8 must be achieved to allow an error of the same size for the calibration of the magnetometer. As the magnetic susceptibilities of dia- and weakly paramagnetic materials are of the order 1 ppm, all objects in the vicinity of the storage volume like the vacuum chamber and the detectors for the decay electrons will inevitably change the magnetic field in the region of interest by several ppm. For this reason, the development of the field measurement system includes the design of a compact, vacuum compatible version of the magnetometer which is capable of measuring the magnetic field in the storage region inside the vacuum chamber after the complete assembly of the experiment.

The magnetometer presented here is based on pulsed NMR [5,6]. The background of the pulsed NMR technique will be discussed here only as far as it is relevant for the construction of a magnetometer. Especially, we will restrict ourselves to the case of nuclei which carry spin $I = \frac{1}{2}$, like the proton. In an external field B_0 such a nucleus can occupy two distinct eigenstates separated in energy by

$$\Delta E = \hbar\omega_L , \qquad \omega_L = \gamma_I B_0 , \tag{1}$$

where ω_L is the *Larmor frequency*, γ_I the *gyromagnetic ratio* of the respective nucleus and $\hbar$ the Planck constant. For a free proton, the gyromagnetic ratio is $\gamma_p = 2\pi$ 42.577469(13) MHz/T [7].

Despite the quantum mechanical nature of the NMR effect, the time evolution of the signal observed in pulsed NMR experiments can often be described by classical

* Corresponding author. Tel. +49 6221 549 222, fax +49 6221 475 733, e-mail prigl@physi.uni-heidelberg.de.

[1] Present address: Brookhaven National Laboratory, AGS, Upton, NY 11973, USA and Physics Department, Yale University, New Haven, Ct 06520-8121, USA.

PII S0168-9002(96)37493-9

equations [5]. This is possible because the signal arises from a huge number of individual magnetic moments. In thermal equilibrium, the magnetic moments $\boldsymbol{\mu}_i$ of the nuclei in a sample add up to a static macroscopic magnetic moment $\boldsymbol{M} = \Sigma_i \boldsymbol{\mu}_i$ which is parallel and proportional to the applied field $\boldsymbol{B}_0$. The behaviour of $\boldsymbol{M}$ under the influence of rf-pulses of frequency $\omega \approx \omega_L$ is best described in a coordinate system S^r rotating relative to the laboratory frame S with the frequency ω about the direction of $\boldsymbol{B}_0$. In S^r, the external field is reduced to $B_0 - \omega/\gamma_l$ which is very much smaller than B_0 if $\omega \approx \omega_L$. If an additional field $\boldsymbol{B}_1$, orthogonal to $\boldsymbol{B}_0$ and static in S^r, e.g. parallel to the x^r-axis, is applied, the magnetic moment $\boldsymbol{M}$ rotates in S^r about an effective magnetic field $\boldsymbol{B}_{\text{eff}} = \boldsymbol{B}_1 + \boldsymbol{B}_0(1 - (\omega/\omega_L))$ (see Fig. 1). In resonance, $\omega = \omega_L$, the effective field is equal to $\boldsymbol{B}_1$ and thus orthogonal to $\boldsymbol{B}_0$, and $\boldsymbol{M}$ rotates with the frequency $\omega_1 = \gamma_l B_1$ about the x^r-axis. If $\boldsymbol{B}_1$ is switched on only for a finite time interval t_p, $\boldsymbol{M}$ is tilted by an angle

$$\alpha = \gamma_l B_1 t_p . \tag{2}$$

In the laboratory frame, the field $\boldsymbol{B}_1$ is a circularly polarized field with angular frequency ω. If it is switched on for a time interval $t_p = (\pi/2)/\omega_1$, the magnetization is effectively tilted by 90° and subsequently precesses with the Larmor frequency ω_L about $\boldsymbol{B}_0$. To completely describe the time evolution of $\boldsymbol{M}$, relaxation effects, i.e. the forces driving the magnetization back to its thermal equilibrium value, must be included. Phenomenologically, the dynamic behavior of $\boldsymbol{M}$ including relaxation is described by the *Bloch equations* [8]

$$\frac{dM_z}{dt} = \gamma_l(\boldsymbol{M} \times \boldsymbol{B}_0)_z - \frac{M_z - M_0}{T_1} = \frac{M_0 - M_z}{T_1},$$
$$\frac{dM_{x,y}}{dt} = \gamma_l(\boldsymbol{M} \times \boldsymbol{B}_0)_{x,y} - \frac{M_{x,y}}{T_2}, \tag{3}$$

where the *transversal* relaxation time T_2 is the time constant for the decay of the component of $\boldsymbol{M}$ *orthogonal* to $\boldsymbol{B}_0$ while the *longitudinal* relaxation time T_1 is the time constant with which the component *parallel* to $\boldsymbol{B}_0$ approaches its thermal equilibrium value $\boldsymbol{M}_0$. The width $\Delta\omega_{1/2}$ of the resonance line (FWHH) is directly related to the transversal relaxation time T_2, e.g., $\Delta\omega_{1/2} = 2/T_2$ for a Lorentzian line. The relaxation times for the proton magnetization in pure water at room temperature are $T_1 = T_2 \approx 3$ s [9], corresponding to a linewidth $\Delta\omega_{1/2}$ of $2\pi \times 0.1$ Hz. In a field of 1.45 T, $\omega_L = 2\pi \times 61.7$ MHz, the quality factor of this resonance line is $\omega_L/\Delta\omega_{1/2} = 6 \times 10^8$ and reflects the extremely high resolution potential of NMR magnetometers and their usefulness for the new $g_\mu - 2$-experiment.

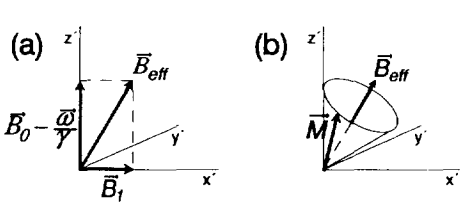

Fig. 1. Effective magnetic field $\boldsymbol{B}_{\text{eff}}$ (a) and magnetic moment $\boldsymbol{M}$ (b) during an rf-pulse in a coordinate system S^μ rotating with the rf frequency ω about the direction of the external field $\boldsymbol{B}_0$. $\boldsymbol{B}_1$ is the magnetic field produced by the rf-pulse.

2. The pulsed NMR magnetometer

A block diagram of the magnetometer is shown in Fig. 2. A low phase noise *synthesizer*, stabilized by a Loran C receiver to 10^{-11} relative accuracy, is the input of a custommade two stage 10 W class C transistor *pulse amplifier* (R. Umathum, Heidelberg, Germany) with a gain of 60 dB, a center frequency of 60 MHz and a bandwidth of 30 MHz. Triggered by the VME computer, the pulse amplifier delivers pulses of about 4 μs duration. After running through the *duplexer* and the *multiplexer*, they produce a linearly polarized rf-field B_1 of about 2 mT in the coil L_S, one of whose circularly polarized components tilts the magnetization of the protons in a water sample by 90°. The homebuilt *multiplexer* (Fig. 3) allows to serve up to 20 probes with a single magnetometer. Each switch consists of two PIN diodes (MAP1250) separated by a $\lambda/4$ line realized with SMD coils and capacitors. A switch is closed by running a current of 7 mA through each of the two PIN diodes. Each open switch represents a capacitance of about 1.5 pF (the capacitance of the MAP1250 diode) parallel to the capacitor C_1 of the $\lambda/4$ line. By lowering the value of C by about 30 pF, we were able to keep the insertion loss of the multiplexer as low as the one of a single switch while retaining an isolation of better than 65 dB of an open switch.

Following the rf-pulse, the precessing component of the proton magnetization induces a voltage with the Larmor frequency ω_L in the coil L_S. This voltage is refered to as the NMR signal. In order to increase the signal amplitude, the coil is part of a resonance circuit with a quality factor Q of about 30. The parallel coil L_p is used to match the circuit to the line impedance of 50 Ω. After running through the multiplexer, the NMR signal is steered by the *duplexer* to the input of a low noise *preamplifier*. The *duplexer* is a nonlinear device separating the transmitter from the receiver. As its bandwidth is of no concern for this magnetometer, the simple, purely passive but very effective design shown in Fig. 4 was chosen. The nonlinear elements are pairs of crossed diodes which represent a short circuit for the strong rf-pulses but a high impedance for the weak NMR signal. For this signal the two $\lambda/4$ lines combine to a single $\lambda/2$ line allowing a free choice for the impedance Z_L. A high value of Z_L was chosen to reduce the voltage at the preamplifier input during the 10 W pulse and thus the deadtime of the receiver.

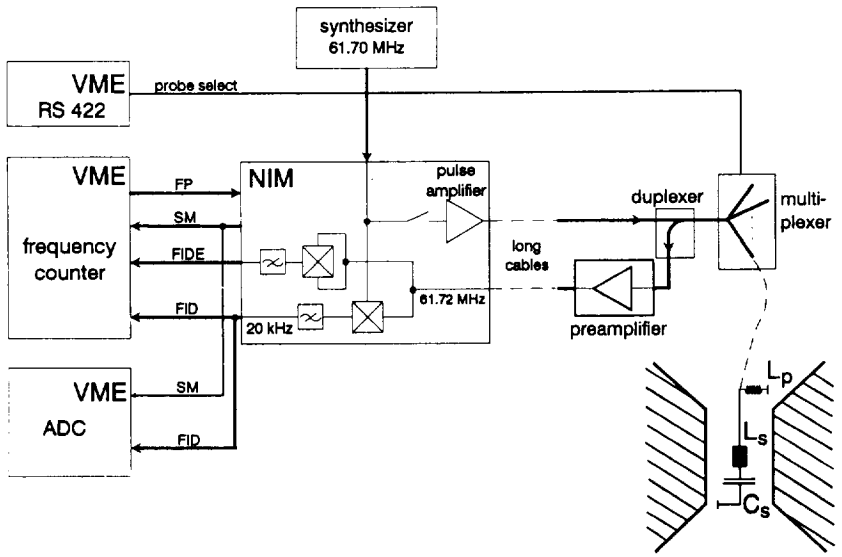

Fig. 2. Block diagram of the pulsed NMR magnetometer. The rf-pulses are produced by a 10 W pulse amplifier. The amplified NMR signal is mixed with the synthesizer frequency to obtain the low frequency FID. A frequency counter, which is read out by a VME computer, measures the FID frequency. The envelope of the NMR signal is used to determine the measuring time. The full FID may be digitized with a 12-bit ADC with selectable sampling rates. The digitized FID may be Fourier transformed to monitor the field distribution over the sample volume.

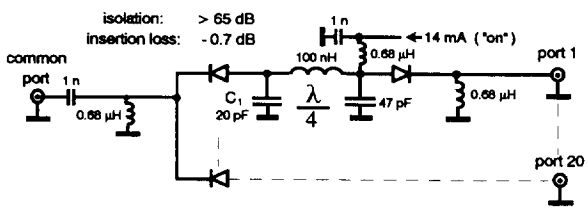

Fig. 3. The 1:20 PIN diode multiplexer. A switch is closed by running a current of 7 mA through each of the two PIN diodes. The two diodes are separated by a $\lambda/4$ line to improve the isolation of an open switch. The $\lambda/4$ is realized with lumped components.

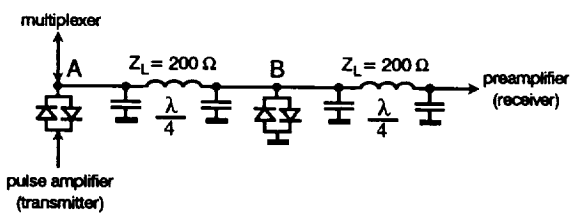

Fig. 4. The duplexer. During the 10 W transmitter pulse, the pairs of crossed diodes represent a short circuit. The $\lambda/4$ line between A and B transforms the short circuit at point B to a high impedance at point A. For the weak NMR signal, the high impedance of the diodes decouples the transmitter from the multiplexer and the preamplifier, and the duplexer acts as a pure $\lambda/2$ line between multiplexer and preamplifier.

The amplified NMR signal is mixed with the synthesizer output, a signal of well defined frequency ω_{ref} close to the NMR frequency ω_L. From the mixing products the difference frequency $\omega_L - \omega_{ref}$ is selected by a low pass filter and further amplified. We will refer to this signal in the KHz region as the FID (free induction decay) of the NMR probe. In a second branch of the receiver the envelope of the NMR signal, called FIDE, is determined by multiplying the preamplifier output by itself and discarding the $2\omega_L$ component. Finally the frequency $\omega_{FID} = \omega_L - \omega_{ref}$ of the FID is measured with the *frequency counter*, an integrated circuit board occupying one quarter of a VMEbus compatible Eurocard. Fig. 5 shows the logic and timing diagram of the frequency counter. A logic pulse SM, derived from the transmitter pulse FP, opens an asynchronous gate AGATE about 10 μs after the end of the transmitter pulse. The 10 μs delay accounts for the deadtime of the preamplifier and allows for the decay of the transient response of the low pass filter in the analog part. The analog input signals FID and FIDE are converted to the logical signals FPULS and EPULS, respectively, by means of comparators with a positive threshold for the envelope FIDE and zero threshold for the FID. When AGATE is high, the output GATE of the D-flipflop FF will be set by the next *rising* edge of FPULS and thus by a positive zero crossing of the FID. The GATE signal enables two counters, one of them counting the pulses of a 20 MHz clock (internal or external) and the other the periods of the FID. The frequency measurement is stopped by the *falling* edge of EPULS as soon as the envelope FIDE has fallen below the

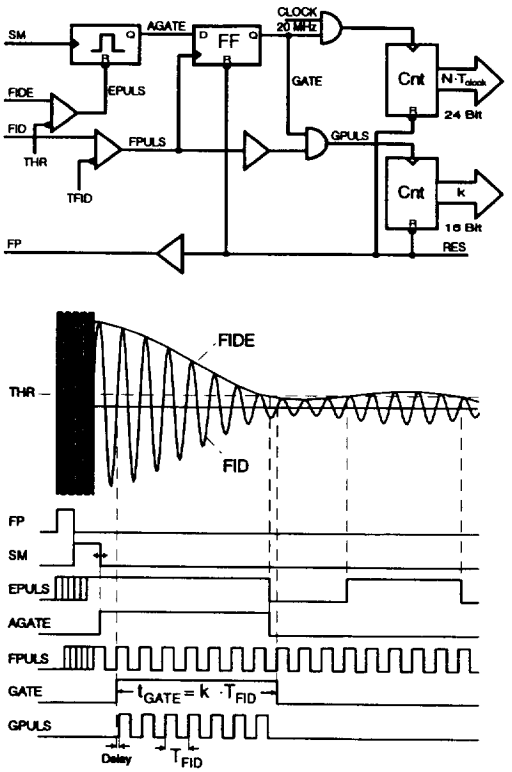

Fig. 5. Frequency counter circuit and timing diagram. The start of the frequency measurement is triggered by the logic pulse SM which is preceded by a pulse FP starting the pulsed excitation. A D-flipflop is used to synchronize the gate signal GATE for the clock counter and the FID period counter with the positive zero crossings of the FID. The end of the measuring time t_{GATE} is derived from the FID envelope FIDE.

threshold of the FIDE comparator. Again, the edge of the counter gate GATE is synchronized to a positive zero crossing of the FID. The measuring time t_{GATE} is thus a known integer multiple k of the FID period. From the time t_{GATE} and this integer k the frequency $\omega_{FID} = 2\pi \times k/t_{GATE}$ is calculated. For long NMR signals, an upper limit for t_{GATE} may be set by the RC time constant of the monoflop. Using Eq. (1) the magnetic field B at the location of the respective probe can be calculated from ω_{FID} as

$$B = \frac{\omega_{ref} + \omega_{FID}}{\gamma_f}. \tag{4}$$

In the $g_\mu - 2$-experiment, almost 400 NMR probes read out by 20 independent magnetometers will be used. The vast majority are 360 fixed probes embedded in the upper and lower plate of the muon vacuum chamber. The design of these probes is shown in Fig. 6. They are housed in grooves machined into the outside surface of the 0.5 in. thick top and bottom aluminium plates of the vacuum

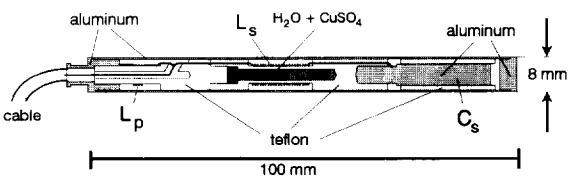

Fig. 6. NMR probe containing a cylindrical water sample. The active water volume has a diameter of 2.5 mm and a length of 15 mm. The cylindrical symmetry was chosen to keep to a minimum the field distortions in the region of the water sample caused by the bulk susceptibility of all parts of the probe. To tune the resonance circuit, the capacitance C_s can be varied by moving a teflon ring in or out.

chamber. Thus all the space between the chamber and the poles of the magnet remains free for the installation of current shims necessary to achieve a field homogeneity of 1 ppm in the muon storage volume [4]. To reduce the relaxation time of the sample, which limits the field measurement repetition rate (see Section 3.5), the probes are filled with a dilute aqueous solution of $CuSO_4$ with a Cu^{2+}-concentration of about 1.5×10^{19} cm^{-3} leading to relaxation times of T_1, $T_2 \approx 30$ ms [10].

3. Characteristics of the pulsed NMR magnetometer

3.1. Accuracy

The field measurement in a pulsed NMR magnetometer is purely passive. The excitation and the detection of the NMR signal are separated in time. Due to the huge number of nuclei contributing to the signal, the voltage induced by the precessing nuclear magnetic moments is virtually free of any statistical error. The dominant noise present is the noise of the circuit needed to pick up the NMR signal, i.e. the Nyquist noise of the 50 Ω resistor represented by the tuned and matched probe circuit.

The accuracy of the FID frequency measurement is

$$\frac{\Delta\omega_{FID}}{\omega_{FID}} = \frac{\Delta t_{GATE}}{t_{GATE}}, \tag{5}$$

where Δt_{GATE} is the uncertainty in the measurement of the time interval $t_{GATE} = k \times 2\pi/\omega_{FID}$. The number of zero crossings k is an integer and does not affect the accuracy. Assuming that the frequency ω_{ref} is known exactly, it follows from $\omega_L = \omega_{ref} + \omega_{FID}$ that $\Delta\omega_L = \Delta\omega_{FID}$ and thus

$$\frac{\Delta\omega_L}{\omega_L} = \frac{\Delta\omega_{FID}}{\omega_{FID}}\frac{\omega_{FID}}{\omega_L} = \frac{\omega_{FID}}{\omega_L}\frac{\Delta t_{GATE}}{t_{GATE}}. \tag{6}$$

Assuming a typical value of $\omega_{FID} = 2\pi \times 30$ kHz, the accuracy required for the measurement of t_{GATE}, and therefore, of ω_{FID} is reduced by a factor of $\omega_L/\omega_{FID} = 2 \times 10^3$ with respect to the field measurement itself! The time

interval t_{GATE}, during which the frequency of the FID is measured, is typically of the order of 1 ms. Changes in the phase of the synthesizer output signal during t_{GATE} lead to an error in the FID frequency. In our field measurements we found that this contribution to the relative uncertainty can be kept well below 10^{-8} if a low phase-noise synthesizer such as the PTS160 (Programmed Test Sources, Inc., MA, USA) is used. Assuming a highly stable reference frequency, the uncertainty Δt_{GATE} arises from two sources.

(a) The time interval t_{GATE} is measured by counting the pulses of a 20 MHz clock, i.e. it is measured in multiples of $T_{clock} = 50$ ns. In a series of measurements the mean error is $\langle \Delta t_{GATE} \rangle = \frac{1}{3} T_{clock}$ [11] resulting in

$$\frac{\Delta\omega_L}{\omega_L} = \frac{\omega_{FID}}{\omega_L} \frac{T_{clock}}{3\, t_{GATE}}. \tag{7}$$

For $t_{GATE} = 1$ ms, $\omega_{FID} = 2\pi \times 30$ kHz and $\omega_L = 2\pi \times 62$ MHz eq. (7) yields

$$\frac{\Delta\omega_L}{\omega_L} = 7.9 \times 10^{-9}. \tag{8}$$

For smaller frequencies $\omega_{FID} < 2\pi \times 30$ kHz, or longer measuring times $t_{GATE} > 1$ ms, the error will be even smaller.

(b) Due to noise $N(t)$, the zero crossings of the receiver voltage

$$U(t) = s(t) + N(t) = S(t_{GATE}) \sin[\omega_{FID} t + \phi] + N(t) \tag{9}$$

do not occur exactly at the zero crossings of the pure FID $s(t)$ but somewhat before or after. $S(t)$ in Eq. (9) is the envelope of the signal $s(t)$. For this magnetometer, in a field of $B \approx 1.45$T, the signal-to-noise ratio S/N is above 300 at the beginning of the time interval t_{GATE} and the measurement is stopped at $S/N \approx 100$. Therefore we can restrict ourselves considering the end of the time interval t_{GATE}. Near the last zero crossing, the receiver voltage can be approximated by

$$U(t_{GATE} + \tau) \approx S(t_{GATE})\, \omega_{FID}\, \tau + N(t_{GATE}) \quad \left(\tau \ll \frac{2\pi}{\omega_{FID}}\right), \tag{10}$$

where we assume that the noise signal is approximately constant in the short time interval during which the signal voltage is comparable to the noise level. As the FID is the output of a low pass filter, there is no high frequency noise present. Assuming Gaussian noise, the zero crossing will occur with 68% confidence while

$$-\frac{S(t_{GATE})}{[S/N]_{t=t_{GATE}}} \leqslant s(\tau) \leqslant \frac{S(t_{GATE})}{[S/N]_{t=t_{GATE}}}, \tag{11}$$

$$\frac{1}{[S/N]_{t=t_{GATE}}} \frac{1}{\omega_{FID}} \leqslant \tau \leqslant \frac{1}{[S/N]_{t=t_{GATE}}} \frac{1}{\omega_{FID}}, \tag{12}$$

where $s(\tau) := S(t_{GATE})\, \omega_{FID}\, \tau$ is the approximate signal for $t \approx t_{GATE}$, $\tau = t - t_{GATE}$, and $[S/N]_{t=t_{GATE}} := S(t_{GATE})/\sqrt{\langle N^2(t) \rangle}$ is the signal to noise ratio at $t = t_{GATE}$. The corresponding standard deviation is

$$\Delta t_{GATE} = \frac{1}{[S/N]_{t=t_{GATE}}} \frac{1}{\omega_{FID}}. \tag{13}$$

Inserting Eq. (13) into Eq. (6) yields

$$\frac{\Delta\omega_L}{\omega_L} = \frac{\omega_{FID}}{\omega_L} \frac{\Delta t_{GATE}}{t_{GATE}} = \frac{1}{[S/N]_{t=t_{GATE}}} \frac{1}{\omega_L\, t_{GATE}}. \tag{14}$$

In contradistinction to the uncertainty resulting from the time resolution of the 20 MHz clock, Eq. (7), the error due to noise is independent of ω_{FID}. Inserting $\omega_L = 2\pi \times 62$ MHz, $t_{GATE} = 1$ ms (as above) and, realistically, $[S/N]_{t=t_{GATE}} = 100$ into Eq. (14) leads to

$$\frac{\Delta\omega_L}{\omega_L} = 2.5 \times 10^{-8}. \tag{15}$$

Due to the long intrinsic relaxation time of the water sample, the duration of the NMR signal will in practice be limited by the field inhomogeneity across the sample volume. A nonuniform field distribution of width δB results in a spread of Larmor frequencies $\delta\omega_L = \gamma_l\, \delta B$ and thus in a loss of coherence with a time constant $\delta t \approx 1/\delta\omega_L$. If the signal decay is dominated by the field inhomogeneity, the envelope of the NMR signal is given by the Fourier transform of the field distribution and the time constant δt is equivalent to the transversal relaxation time T_2 and thus to the measurement time t_{GATE}. Consequently, the accuracy of the magnetometer depends on the field homogeneity in the sample volume. In our examples we used $t_{GATE} = 1$ ms corresponding to a spread of the Larmor frequencies of $2\pi \times 300$ Hz or 5 ppm out of $\omega_L = 2\pi \times 62$ MHz. According to Eq. (15) we are able to measure this 5 ppm field spread in the sample volume to an accuracy of 0.5%.

Although the gyromagnetic ratio γ_l does not affect the relative accuracy of the field measurement, the knowledge of its absolute value actually is the limiting factor for determining the strength of the field B. It should be noted that γ_l is treated as a bulk constant of the complete NMR probe rather than the value of the single free nucleus (proton). In the latter case, γ_l would be a fundamental constant, but Eq. (4) would only yield the value of the average magnetic field at the positions of the nuclei. This average field deviates from the external magnetic field due to the screening effect of the electrons surrounding the nuclei, known as the chemical shift [6], and, in addition, by the field distortions caused by the bulk susceptibility of all parts of the NMR probes including the (water) sample [12].

For the $g_\mu - 2$-experiment, and in general for all experiments measuring magnetic moments of elementary par-

ticles, it is appropriate to define the magnetic field by the Larmor frequency ω_p of a free proton, $B := \omega_p/\gamma_p$. In this case, the determination of γ_i is equivalent to the measurement of the ratio between the gyromagnetic ratio of the probe and that of a free proton. For protons in a spherical water sample, this ratio is known to an accuracy of 0.014 ppm from the combined results of two sophisticated experiments [13,14]. Thus, for the calibration of the NMR probes, which must be done with a relative accuracy of 5×10^{-8}, a spherical sample can be used.

3.2. Measurable range of magnetic field

For the magnetometer shown in Fig. 2, the measurable range of the magnetic field is limited by the bandwidth of the resonance circuit of the probe. The probes built for the $g_\mu - 2$-experiment (Fig. 6) have a quality factor of $Q \approx 30$ corresponding to a bandwidth of 3% and this is also the range in which a magnetic field can be measured without retuning the probes. As an NMR magnetometer derives the field information from a resonance signal, it is also important to specify the size of field variations that can be tolerated without losing the resonance. This feature is important whenever the magnetometer has to be able to follow small, fast field changes. Typical causes of such field changes are (1) movements of a probe in an inhomogeneous field, e.g., when mapping a field in a large volume with a single probe, (2) small-amplitude field modulations, or (3) switching between different probes in a multiple-probe system. The range of fields a pulsed NMR magnetometer is sensitive to at the same time, i.e., for a fixed synthesizer frequency ω_{ref}, is limited either by the bandwidth of the rf-pulse or by the width of the low pass filter following the mixer (see Fig. 2). The rf-pulse bandwidth is related to the pulse length and thus, indirectly, to the output power of the pulse amplifier. In our case, the length of a 90°-pulse (Eq. (2)) is about 4 μs. This implies a reduction of about 10% of the rf amplitude for an offset of 100 kHz (0.16% out of 62 MHz). With respect to the frequency range the magnetometer is sensitive to for a given synthesizer frequency, the rf-pulse bandwidth is by far more restrictive than the bandwidth of the probes. It could be increased by either using an amplifier with a higher output power or by reducing the length of the rf-pulse. The latter option would imply sacrificing the optimum flip angle of $\boldsymbol{M}$ and thus would result in a decrease of the S/N-ratio.

In general, it is preferable not to be limited by the available rf-power but by the bandwidth of the low pass filter. The signal-to-noise ratio of the FID can then be optimized by adjusting the filter bandwidth to the frequency range that actually has to be covered by the magnetometer. Within the bandwidth of the filter, the pulsed NMR magnetometer is sensitive to any field value at any time. In this sense, the magnetometer, although using a sample with a single resonance line, indeed exploits the great virtue of the pulsed NMR technique, namely its ability to record different resonance frequencies simultaneously.

3.3. Tolerable field gradient

In order to record at least one full period of the FID, a minimum length of the transient signal of about 30 μs is required for $\omega_{FID} \approx 2\pi \times 30$ kHz. This sets a lower limit of about the same size to the tolerable relaxation time T_2. Assuming a Gaussian field distribution in the sample volume, a value of T_2 of 30 μs corresponds to a field distribution with a width of $\Delta B = 2\sqrt{2}\, B_0/(\omega_L T_2) \approx$ 0.35 mT or 250 ppm out of 1.45 T. The relative accuracy of a single measurement is then, according to Eq. (14) with $t_{GATE} = T_2$, roughly 1 ppm. To achieve a precision of 5×10^{-8} the tolerable field spread in the sample volume is about 10 ppm. For the probes shown in Fig. 6, the field gradient is thus limited to 50 ppm/cm in the transverse and 10 ppm/cm in the axial direction of the probe. In general it is preferable to make the sample diameter D as large as possible, because the sample volume and thus the FID amplitude is proportional to D^2 (D^3 in case of a spherical sample) whereas the length of the FID scales with D^{-1}.

3.4. Repetition rate of field measurements

The minimum time interval between subsequent field measurements is given by the longitudinal relaxation time T_1 which, in the case of an aqueous solution of paramagnetic ions, can be adjusted in a wide range (1 ms–3 s) by the concentration of the ions. The best performance of a magnetometer reading out a single probe is achieved if T_1 is roughly equal to the upper limit of the transversal relaxation time T_2 which is set by the local field inhomogeneity at the position of the probe. A relaxation time of 30 ms of the $CuSO_4$-solution in our probes was chosen to allow a precision of one part in 10^8 in a single measurement as well as to be able to accumulate a series of measurements for selected probes within the time constant of the magnetic field regulation which is typically several seconds.

4. Performance test of the magnetometer

The performance of the magnetometer was extensively tested in a superconducting solenoid which is part of a muonium hyperfine structure experiment [15] at the Clinton P. Anderson Meson Physics Facility (LAMPF) in Los Alamos, USA. The field in this solenoid is 1.7 T corresponding to a Larmor frequency of $\omega_L = 2\pi \times 72.3$ MHz. Although designed as a narrowband instrument optimized for a field of 1.45 T, the magnetometer could be used for

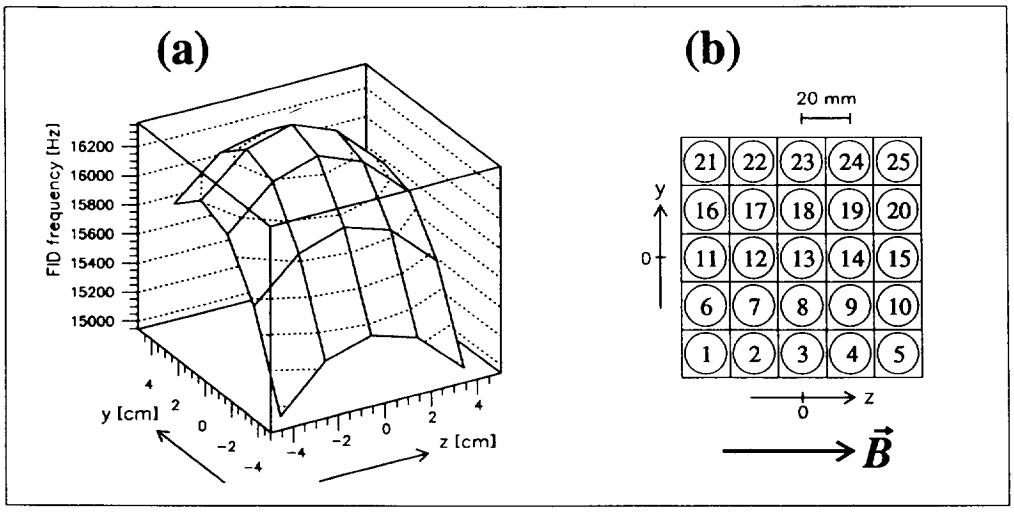

Fig. 7. (a) Field map taken in a large-bore superconducting MRI magnet. A matrix of 25 probes was used covering a cross section of $8 \times 8\,\mathrm{cm}^2$. The FID frequencies spread over a range of 1400 Hz corresponding to a field inhomogeneity of 20 ppm. The synthesizer (reference) frequency was set to $\omega_{\mathrm{ref}} = 2\pi \times 72.3$ MHz and $\omega_{\mathrm{L}} = \omega_{\mathrm{ref}} + \omega_{\mathrm{FID}}$. The positions of the probes in the matrix and the direction of the magnetic field are indicated in (b).

field measurements at 1.7 T with only retuning the NMR probes to the higher frequency.

In Fig. 7a a map of the magnetic field near the center of the magnet prior to shimming is shown. The relatively poor field homogeneity of 1000 ppm in a 50 cm diameter spherical volume at that time was due to the effect of the iron case which is needed to shield the solenoid from its environment and vice versa. The map was taken with a set of 25 probes, arranged in a $8 \times 8\,\mathrm{cm}^2$ matrix (Fig. 7b). For the test measurements, probes with a 5 mm glass tube sample (inner diam. 4.2 mm) and a length of the coil L_S of 6 mm were used. The active water volume and thus the FID amplitude was therefore similar to that of the probe shown in Fig. 6. The shape of the sample volume, however, was better suited for the truely three-dimensional field distribution in the large-bore solenoid. Fig. 8 shows the digitized FIDs of four of the 25 probes. They demonstrate the dependence of the length of the FID on the field homogeneity. It is best at probe #18 which was located near the saddle point of the field. The initial signal-to-noise ratio is 320:1. Although the length of the signals and thus the measuring time t_{GATE} varied between 5 and 15 ms, the standard deviation of a great number of frequency measurements from their mean $\bar{\omega}/2\pi$ in the constant field of the solenoid was initially similar for all probes, improving merely from $\sigma_1 = 1.2$ Hz for probe #1 to $\sigma_{18} = 0.8$ Hz for probe #18. The accuracy of the measurements was actually limited by the phase-noise of the synthesizer Fluke 6160A used at the time of these tests. Later on, this synthesizer was replaced by a PTS160 synthesizer and a standard deviation of 0.25 Hz or 3.5 parts in 10^9 out of 72.3 MHz was obtained for the probes in the most homogeneous region of the field.

For a given bandwidth of the resonance circuit, the signal amplitude of an NMR probe is proportional to ω_{L}^2, respectively B_0^2 [16], and thus one would expect the S/N ratio in the 1.7 T field to be significantly higher than in the 1.45 T field, the magnetometer was designed for. However,

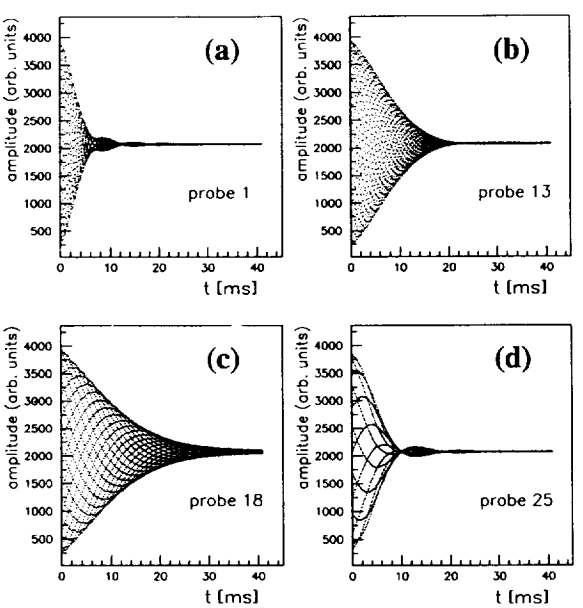

Fig. 8. Digitized free induction decay (FID) signals of probes 1 (a), 13 (b), 18 (c) and 25 (d) in the setup of Fig. 7. The signals were recorded with a 12 bit ADC at a rate of 100 kHz. Each signal consists of 4 k data points. The apparent structures in the signals arise from the small ratio between the digitizing rate and the signal frequencies.

in the NMR probes used, the resistance of the resonance circuit, dominated by the rf absorption of the water sample, is frequency dependent and the quality factor increases with decreasing frequency. This results in a fairly constant signal amplitude over a wide frequency range.

After the installation of an iron shimming kit in the solenoid, a field homogeneity of 0.6 ppm over a 20-cm diameter sphere was achieved. In subsequent measurements, the field distribution in the sample volume of the NMR probes was no longer dominated by the external field inhomogeneity but by the field distortions caused by the dia- and paramagnetic parts of the probe. These field distortions mainly result in a shift of the NMR frequency which can be accounted for by calibrating the probe against a standard. However, if the field distribution is not symmetric, the frequency of the decaying FID is not constant but varies as a function of time. As an illustrative example, a probe with a spherical sample of water is shown in Fig. 9. The sample is contained in a commercial spherical glass bulb (Wilmad Glass Company, NJ, USA) with an inner diameter (ID) of 3 mm which is blown upon a 1 mm ID capillary. To avoid the development of an air or water vapor bubble in the spherical part, the whole capillary has to be filled with water. The water in the capillary causes a distortion of the magnetic field in the spherical part of the sample and in addition contributes, although only to a very small extent, to the NMR signal. Fig. 10 shows the FID and the resonance line of one of these probes. The probe axis was aligned orthogonal to the magnetic field direction resulting in higher resonance frequencies towards the capillary due to the diamagnetic bulk susceptibility of water. Consequently, the resonance line is broadened towards higher frequencies and spreads over a range of about 2 ppm. The frequency of the FID is therefore not constant but moves by roughly 0.1 ppm from its initial value, given by the center of mass of the resonance line, towards the line maximum due to the shorter decay times of the contributions from the less homogeneous region. With regard to the frequency measurement, this implies that the output of the frequency counter depends on the measuring time t_{GATE}. The same argument applies to asymmetric field distributions caused by materials in the immediate vicinity of the probe.

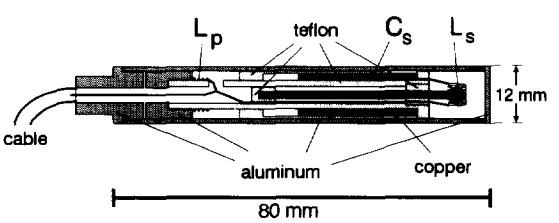

Fig. 9. NMR probe with a spherical water sample. As for the probe in Fig. 6, a variable capacitor to ground is used to tune the resonance circuit.

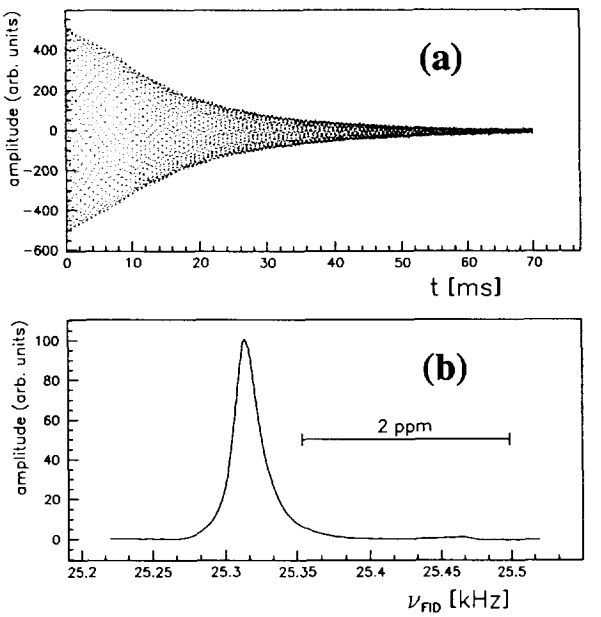

Fig. 10. FID signal (a) of a probe with a spherical water sample (Fig. 9) and its Fourier transform (b). The shape of the resonance line reflects the field inhomogeneity in the active water sample, the long tail to the right being caused by the water column in the capillary.

The dynamic frequency shift caused by the bulk susceptibility of the sample can be avoided by using a solution with vanishing susceptibility. For an aqueous solution of $NiCl_2$, e.g., the transition from dia- to paramagnetic behavior occurs at a concentration of roughly 0.15 Mol/l. In this *zero susceptibility* solution, the relaxation time T_2 is reduced to about 7 ms which, according to Eq. (15), is still long enough to allow measurements to a relative accuracy of better than 10^{-8}. On the other hand, the reduced relaxation time clearly limits the measurement accuracy. To achieve a precision of one part in 10^9 or better, the bulk susceptibility effects have to be further reduced by a more sophisticated probe design. With respect to absolute field measurements the accuracy is currently not limited by the precision of the magnetometer but rather by the uncertainties in the fundamental constants involved and an improvement in their knowledge is required to fully exploit the resolution potential of NMR magnetometers.

Acknowledgements

The authors would like to thank the colleagues in our workshops for their valuable assistance in the design and construction of the magnetometer and the members of the new $g-2$ collaboration, lead by V.W. Hughes, W. Morse and B.L. Roberts, for their continuous interest and encouragement. The work has been supported by the German

Bundesminister für Bildung und Forschung (BMBF), by a NATO Research Grant, and by a Feodor Lynen Fellowship of the Alexander von Humboldt Foundation (R.P.).

References

[1] J. Bailey et al., Nucl. Phys. B 150 (1979) 1; W. Rüegg et al., Phys. Rev. D 25 (1982) 652; F.G. Mariam et al., Bull. Am. Phys. Soc. 27 (1982) 480; K. Weyand and G.D. Willenberg, IEEE Trans. Instrum. Meas. 36 (1987) 275; M.V. Gorshkov et al., Sov. Phys. Dokl. 34 (1989) 362.

[2] B. Adeva et al., Nucl. Instr. and Meth. A 289 (1990) 35; ALEPH Collaboration, Nucl. Instr. and Meth. A 294 (1990) 121.; D. Newton, Proc. CERN Accelerator School, Montreux 1992, ed. S. Turner (CERN 92-05, Geneva, 1992) p. 283.

[3] V.W. Hughes, in: Gift of Prophecy, ed. E.C.G. Sudarshan (World Scientific, 1995) p. 222; B.L. Roberts, Z. Phys. C 56 (1992) S101.

[4] G.T. Danby and J.W. Jackson, IEEE Trans. Appl. Supercond. 5 (1995) 662.

[5] A. Abragam, The Principles of Nuclear Magnetism (Oxford University Press, 1961).

[6] C.P. Slichter, Principles of Magnetic Resonance, 3rd ed. (Springer, Berlin, 1990).

[7] E.R. Cohen and B.N. Taylor, Rev. Mod. Phys. 59 (1987) 1121.

[8] F. Bloch, Phys. Rev. 70 (1946) 460.

[9] J.H. Simpson and H.Y. Carr, Phys. Rev. 111 (1958) 1201.

[10] R.A. Bernheim et al., J. Chem. Phys. 30 (1959) 950.

[11] R. Prigl, doctoral thesis, University of Heidelberg (1994).

[12] K. Borer and F. Lange, Nucl. Instr. and Meth. 143 (1977) 219.

[13] P.F. Winkler et al., Phys. Rev. A 5 (1972) 83.

[14] W.D. Phillips et al., Metrologia 13 (1977) 179.

[15] M.G. Boshier et al., Phys. Rev. A 52 (1995) 1948.

[16] U. Haeberlen, NMR Basic Principles and Progress 25 (1990) 143.